J. Fluid Mech. (1970), *vol.* 43, *part* 2, *pp.* 247–255
Printed in Great Britain

The motion of large bubbles in horizontal channels

By G. C. GARDNER AND I. G. CROW
Central Electricity Research Laboratories, Leatherhead, Surrey

(Received 9 December 1969)

An experimental investigation of a large long air bubble moving into stationary water in a horizontal channel of rectangular cross-section is presented and three well-defined flow régimes for the water discharged beneath the bubble are described. The influence of surface tension on the bubble velocity is explained using the hypothesis that the radius of curvature of the two-phase interface close to the upper wall does not vary greatly with channel depth and is close to the theoretical value for a channel of such depth that the bubble is just motionless.

1. Introduction

The propagation rate of large bubbles in vertical tubes has received considerable attention in the last decade, largely because of its value in interpreting the two-phase 'slug flow' régime. White & Beardmore (1962) demonstrated that the dimensionless groups which successfully correlate experimental information, if the light phase viscosity can be ignored, are a Froude number

$$F_d = \left[\frac{u^2}{gd}\frac{\rho}{\Delta\rho}\right]^{\frac{1}{2}}, \tag{1.1}$$

an Eötvös number,

$$\Sigma_d = \frac{4\sigma}{\Delta\rho g d^2}, \tag{1.2}$$

and a physical property group

$$P = \frac{g\mu^4\Delta\rho}{\rho^2\sigma^3}, \tag{1.3}$$

where u is the bubble velocity relative to the liquid ahead of it, g is the gravitational constant, d is the tube diameter, ρ is the heavy phase density, $\Delta\rho$ is the density difference between the heavy and light phases, σ is the surface tension and μ is the heavy phase viscosity.

It was shown that the liquid phase viscosity, however, has negligible influence if P is less than 10^{-8}, which is true for the air–water system used in the present work. In that event F_d achieves an essentially constant value of slightly less than 0·35 for $\Sigma_d < 10^{-2}$, in agreement with the theoretical conclusion of Dumitrescu (1943) for inviscid flow without surface tension. On the other hand F_d is zero according to Bretherton (1961), when $\Sigma_d \geqslant 1{\cdot}19$, which substantially agrees with White & Beardmore's experimental result that the bubble blocks the tube for $\Sigma_d \geqslant 1{\cdot}0$.

All the results noted above were obtained for a heavy phase which was stationary with respect to the tube wall upstream of the advancing bubble or

for $u_L = 0$, where u_L is the average heavy phase velocity relative to the wall above the bubble. Nicklin, Wilkes & Davidson (1962), however, showed that, when $u_L \neq 0$, the consequent velocity profile in the heavy phase modifies the momentum flux relative to the bubble in such a manner as to increase the bubble velocity relative to the average fluid velocity above it. Thus, for conditions such that F_d otherwise equals 0·35, this last velocity increases by $0{\cdot}2u_L$.

Experimental results for sloping tubes have been obtained by Runge & Wallis (1965) and Zukoski (1966). Zukoski used two-liquid-phase systems, amongst others, and clearly demonstrated the validity of using $\Delta\rho$ in the fashion shown by (1.1) and (1.2). He also gave a curve of F_d *versus* Σ_d for horizontal tubes, which is useful in confirming the conclusions of the present paper.

A theory for large long bubbles in horizontal channels was given by Benjamin (1968). He examined the inviscid flow without surface tension and found that $F = [u^2/gh]^{\frac{1}{2}}(\rho/\Delta\rho)^{\frac{1}{2}} = 0{\cdot}5$ for a system of parallel horizontal surfaces, while for a tube of circular cross-section $F_d = 0{\cdot}542$, in substantial agreement with an extrapolation of Zukoski's data.

The present paper describes an experimental investigation of a large bubble of air advancing into stationary water in a horizontal channel of rectangular cross-section. It confirms that Benjamin's result is probably correct for very deep channels but consideration has to be given to the influence of surface tension, at least for channels as deep as 175 mm, which was the deepest used experimentally.

2. Experimental apparatus and observations

The apparatus consisted of a horizontal Perspex channel, 1830 mm long and 100 mm wide, whose top could be moved within the retaining walls to vary the depth from 0 to 175 mm. One end of the channel was closed by a fixed wall while the other was sealed with a flap, hinged at the bottom. Releasing the flap allowed water to discharge freely, as it was displaced by the advancing air bubble.

The channel was carefully cleaned before use, but it was none the less felt, after the first few runs, that the water might not be satisfactorily wetting the upper Perspex wall. This surface was therefore changed to brass but it made no difference to the measurements, in line with Zukoski's (1966) experience.

The channel was carefully aligned for each change of channel depth and the final, most sensitive check was to ensure that the bubble ran true down the whole length of the channel. The bubble velocity was measured by timing the passage of the nose past markers set 500 and 1000 mm apart. Still photographs and ciné films were taken during separate runs to measure the depth of flow downstream of the bubble nose and to make general observations of the nature of the flow.

Three flow régimes were observed, which are illustrated by the photographs in figure 1, plate 1, and which will be described with reference to the Eötvös number,

$$\Sigma = \frac{4\rho}{\Delta\rho g h^2} \tag{2.1}$$

relevant to rectangular channels. h is the channel depth.

For deep channels, with $\Sigma < 0{\cdot}02$, the flow was much as conceived by Benjamin (1968), except for the curved nose near the top wall. A disturbance in the form of a surface elevation was created by the release of the end flap but it decayed rapidly and the bubble velocity was sensibly constant with respect to distance down the channel.

In the range of Σ from 0·02 to 0·105, large waves formed downstream of the bubble nose, beyond the point at which the bubble attained its maximum depth. These waves kept pace with the bubble and showed little, if any, attenuation. At one value of Σ in this range, however, capillary waves were seen to move slowly towards the bubble nose (see figure 1(*c*)). Again, the bubble velocity did not alter along the channel.

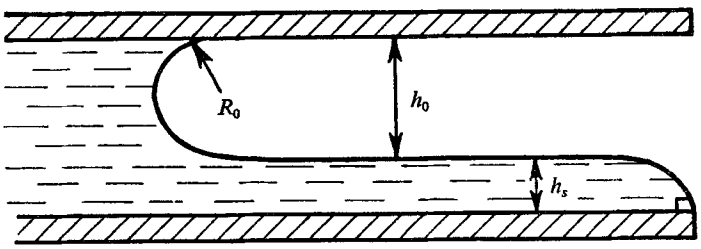

FIGURE 2. The blocked condition, showing undrained water.

For $\Sigma > 0{\cdot}105$ the flow was much more quiescent and the fraction of the channel depth occupied by the liquid downstream of the bubble nose increased. The channel finally blocked and F equalled zero when Σ reached a critical value of $\Sigma_0 = 0{\cdot}368$. This was determined by giving the upper channel wall a slight slope to allow the bubble to advance into a thinning cross-section and halt at the point where the depth was its critical value. Figure 2 illustrates the blocked system, which shows that a substantial layer of water of depth h_s remained undrained from the bottom of the channel. The sill over which the water discharged was square-ended and the water drained until the vertical part of the sill was just wetted or, in other words, the water contacted the end of the horizontal surface at an angle of $\frac{1}{2}\pi$. Some measurements were made with a chamfered sill in an attempt to induce better drainage but drainage was never perfect.

The experimental results for the bubble velocity are shown in the F *versus* Σ plot of figure 3. A distinction is made between results obtained with the square-ended and chamfered sills. It is clear that the form of sill had little influence upon the results, except for channels whose depth was close to the critical value for blockage.

The experimental results for the depth of water flow downstream of the bubble nose are given in figure 4 in terms of $H = h_2/h$ and $H_J = h_3/h$ *versus* Σ. h_2 is the minimum depth of flow occurring close to the bubble nose and h_3 is the average depth of flow measured downstream from the first wavecrest following the nose. The three flow régimes discussed above can be distinguished in this figure.

Figure 5 presents bubble nose profiles traced from photographs and a comparison is made with the bubble profile predicted by Benjamin (1968). There is not a close agreement between the theoretical and experimental shapes for a

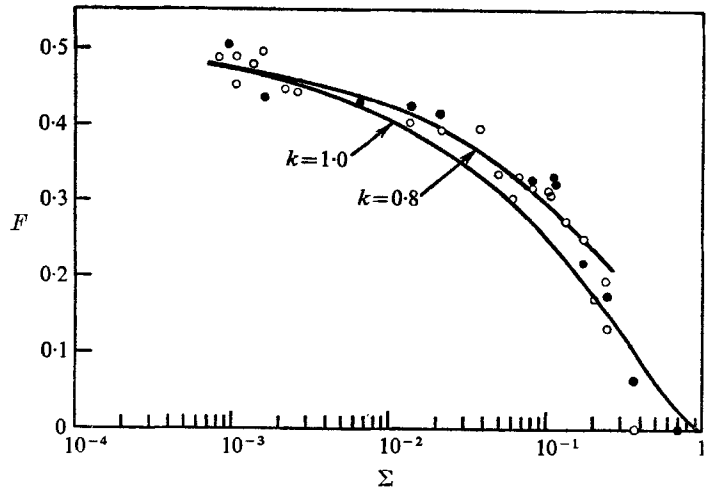

FIGURE 3. Comparison of experimental and calculated values of F for a rectangular channel. ○, square-ended sill; ●, chamferred sill.

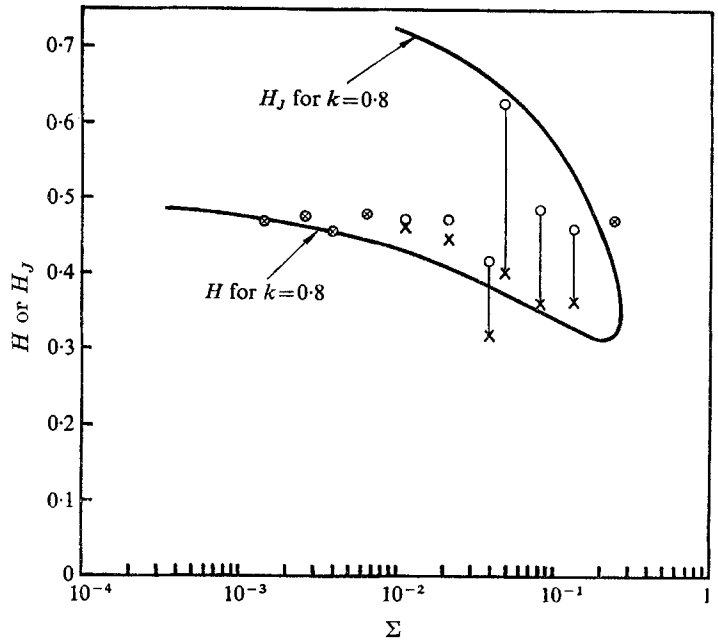

FIGURE 4. Comparison of experimental and calculated values of H and H_J for a rectangular channel. ×, minimum reduced depth; ○, average reduced depth after hydraulic jump.

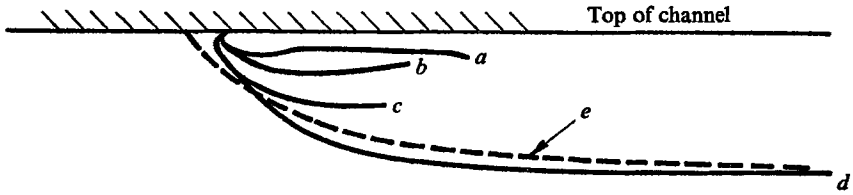

FIGURE 5. Superimposed bubble profiles for four channel depths together with theoretical profile of Benjamin (1968) for a depth of h = 107 mm. *a*, h = 15 mm; *b*, h = 27·5 mm; *c*, h = 60 mm; *d*, h = 107 mm; *e*, h = 107 mm, Benjamin theory.

channel of 107 mm depth, though agreement might not be expected where surface tension still has appreciable influence.

3. Discussion of results

3.1. *Bubble velocity*

Surface tension has a substantial effect upon the bubble velocity for the air–water system in channels as deep as 175 mm. Zukoski (1966) came to the same conclusion with respect to large bubbles in horizontal tubes and it deserves some quantitative explanation. Consider the system illustrated in figure 6 where, for convenience, the bubble is assumed to be held stationary by flowing liquid.

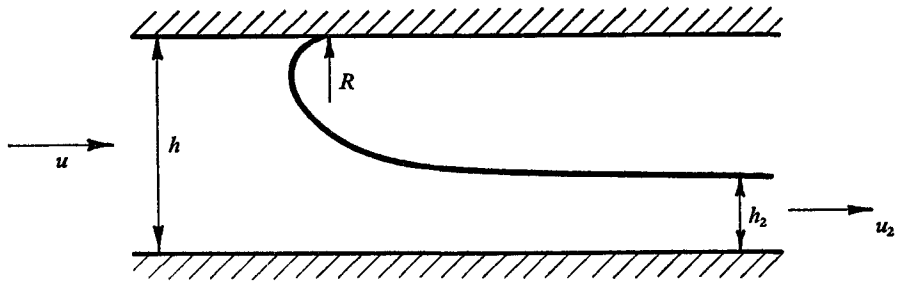

FIGURE 6. Dimensions and velocities.

The upstream velocity is u and the depth of flow h. The downstream velocity is u_2 and the depth of flow h_2. The liquid phase is assumed to wet the upper wall, with a zero contact angle, in preference to the light phase, and the two-phase interface has a radius of curvature of R at its point of contact with the upper wall. Following Benjamin (1968), volumetric, momentum and energy balances are written between a station far upstream and a station sufficiently far downstream for the velocities to be sensibly uniform, but terms involving surface tension are included. To write the balances it is assumed that the point of contact of the two-phase interface with the upper wall is a stagnation point and they are then respectively,

$$uh = u_2 h_2, \tag{3.1}$$

$$\rho u^2 h + \tfrac{1}{2}\rho g h^2 = \rho u u_2 h + [\tfrac{1}{2}\rho u^2 + (\sigma/R) + \tfrac{1}{2} g \rho_L (h - h_2)]\,(h - h_2) + [\tfrac{1}{2}\rho u^2 + (\sigma/R) + g\rho_L (h - h_2) + \tfrac{1}{2}\rho g h_2]\,h_2 - 2\sigma, \tag{3.2}$$

and

$$\tfrac{1}{2}u^2 + gh = \tfrac{1}{2}u^2 + \tfrac{1}{2}u_2^2 + (\sigma/\rho R) + (\rho_L/\rho)\, g(h - h_2) + g h_2, \tag{3.3}$$

where energy losses have been ignored and ρ_L is the light phase density. It is, perhaps, helpful to note that σ/R is the pressure rise over the two-phase interface at the stagnation point and also that the last term of (3.2) comprises the sum of the tension in the interface at the downstream station and the tension in the interface at its point of contact with the upper wall.

Before (3.1) to (3.3) can be solved to obtain useful results we require a value for R, which would be difficult to obtain theoretically for the whole range of Σ. It is noted, however, that the relevant part of the interface is in a region of low

velocity and thus there is a reasonable expectation that R will not vary substantially. Now $R = R_0$ for the critical blocked flow condition can be determined unambiguously by setting $u = u_2 = 0$ in equations (3.1) to (3.3). Equation (3.1) becomes redundant, (3.2) reduces to a simple force balance and (3.3) becomes a statement of pressure equilibrium. Simultaneous solution of (3.2) and (3.3) yields:

$$R_0 = \tfrac{1}{4}h_0 = \tfrac{1}{2}(\sigma/\Delta\rho g)^{\frac{1}{2}} \tag{3.4}$$

or

$$\Sigma_0' = 1. \tag{3·5}$$

A slight difficulty is now noted, that the experimental result was $\Sigma_0 = 0{\cdot}368$ for a square-edge sill, which, however, had an undrained liquid depth on it of h_s, as shown in figure 2. A force and pressure balance, in the same manner as carried out above and assuming a contact angle of $\frac{1}{2}\pi$ with the horizontal surface, yields

$$h_s = (2\sigma/\Delta\rho g)^{\frac{1}{2}}. \tag{3.6}$$

Thus the experimental value of Σ_0 based upon the sum of h_0 of equation (3.4) and h_s of equation (3.6) should equal

$$\Sigma_0 = (1 + 0{\cdot}5^{\frac{1}{2}})^{-2} = 0{\cdot}343. \tag{3.7}$$

Agreement between the theoretical and experimental value is sufficiently close for the value of R_0 of (3.4) to be accepted and to write

$$\sigma/R = K\Delta\rho g h\Sigma^{\frac{1}{2}}, \tag{3.8}$$

where

$$K = k + (1-k)\Sigma^{\frac{1}{2}}, \tag{3.9}$$

and k is an empirical constant. Equations (3.8) and (3.9) merely state that R varies from R_0, given by (3.4), when $\Sigma = 1$ to R_0/k when $\Sigma = 0$. K must be close to unity for the analysis to be of value in interpreting experimental results.

Substitution of (3.1) and (3.8) in (3.2) and (3.3) yields

$$F^2(2-H)/H = 1 - H^2 - 2K\Sigma^{\frac{1}{2}} + \Sigma, \tag{3.10}$$

$$\tfrac{1}{2}F^2/H^2 = 1 - H - K\Sigma^{\frac{1}{2}}. \tag{3.11}$$

Simultaneous solution of these equations, using $k = 1{\cdot}0$ and $k = 0{\cdot}8$, gave the F *versus* Σ curves of figure 3. It is seen that the curve for $k = 0{\cdot}8$ fits the results very well, except for the quiescent flow régime for $\Sigma > 0{\cdot}105$. In any case this curve does not extend beyond $\Sigma = 0{\cdot}275$, for reasons which will become clearer during the discussion of the liquid depth beneath the bubble.

It may be noted in passing that the treatment given above may now be used to estimate the error in employing an experimental channel of finite width to determine the bubble velocity that would be obtained in an infinitely wide channel. It is found that the error in F, for a channel of 100 mm width, has a maximum value of 4 % at $\Sigma = 0{\cdot}1$, if account is taken of the tension in the liquid film wetting the side walls.

The agreement between the treatment and experiment is evidence in favour of the view that R does not vary substantially for the whole experimental range. This is also the impression gained by an inspection of the tracings of the bubble nose shown in figure 5, though they cannot be used for an accurate measure of R.

The treatment must be extended in order to compare it with Zukoski's (1966) results for a tube. First, one must assume that the downstream two-phase interface is plane, though near the blocked condition it must have one radius of curvature almost equal to the tube radius. Secondly, the two-phase interface must have a second principal radius of curvature, besides R, equal to the tube radius at the point where it contacts the upper wall. Lastly (3.4), (3.8) and (3.9) must be reconsidered even though it is found that they remain unaltered. A force balance and pressure equilibrium still yield R_0 given by (3.4), while the flow near the top stagnation point for a very large tube will approximate to the two-dimensional system and thus there is no reason to believe that k will be substantially changed. We get

$$F_d^2 \frac{2A - A_H}{A_H} = \left[1 - \frac{x_H A_H}{xA}\right] - \Sigma_d \left[1 + 2K\Sigma_d^{-\frac{1}{2}} - \frac{aS}{A}\right] \tag{3.12}$$

$$F_d^2 \left[\frac{A}{A_H}\right]^2 = 2[1 - H] - \Sigma_d[1 + 2K\Sigma_d^{-\frac{1}{2}}], \tag{3.13}$$

in place of (3.10) and (3.11). A and A_H are the cross-sectional areas of the tube and of the liquid far downstream respectively. x and x_H are respectively the distance of the centre of pressure of A from the top of the channel and of A_H from the two-phase interface. S is the perimeter of the light phase far downstream and a is the tube radius.

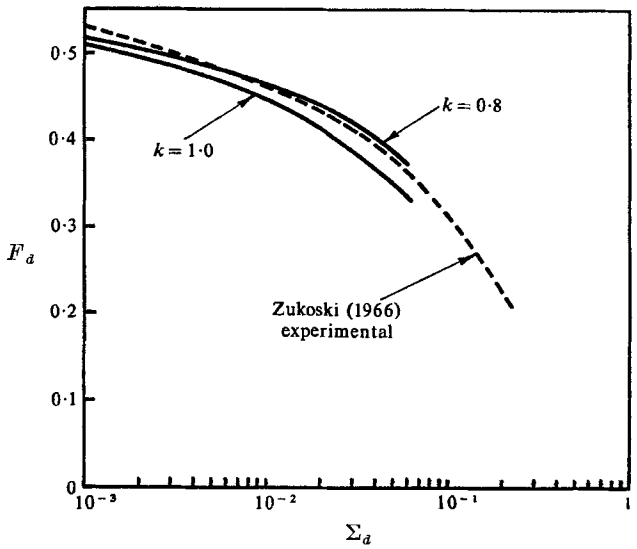

FIGURE 7. Comparison of experimental and calculated values of F_d for a horizontal tube.

Solutions of these equations are shown in figure 7 in comparison with Zukoski's experimental results. Agreement when $k = 0{\cdot}8$ is again excellent, though the curve does not cover the whole experimental range, largely due to the assumption that the downstream interface is plane. It should be noted that Zukoski s results

appear to be tending to a value of F_d which is higher than the theoretical value of 0.542 given by Benjamin for $\Sigma_d = 0$. It is possible that F_d is tending to 0·567, which is the maximum value that could be achieved with energy losses occurring, as discussed by Benjamin (1968). The results are not sufficient, however, to resolve this point.

3.2. *Depth of flow beneath the bubble*

The treatment of the last subsection contained the assumption in (3.3) that the flow was lossless, at least in the region between a station ahead of the bubble and the position of the minimum flow depth near the bubble nose. Measurement of the bubble velocity, however, is an insensitive test of this assumption, as is evident from the discussion of Zukoski's results, and a much better test is provided by the measurement of flow depth beneath the bubble.

Benjamin (1968) showed theoretically that, in the case of two-dimensional bubbles studied here, $F = H = 0{\cdot}5$ for lossless flow when $\Sigma = 0$. Further, as energy losses are increased from zero, F increases to a maximum value of 0·5273 when $H = 0{\cdot}6527$. Simultaneously the Froude number for the flow beneath the bubble and relative to the bubble nose decreases from $\sqrt{2}$ to unity, so that the magnitude of a hydraulic jump travelling with the bubble would be expected to decrease to zero as the maximum value of F was attained. It is readily demonstrated that similar results are to be expected for $\Sigma > 0$ and in particular that the maximum value of F will correspond with a Froude number of unity for flow beneath the bubble.

Figure 4 shows that H tends to approach 0·5 as Σ tends to zero and that it is therefore unlikely that there are substantial energy losses when $\Sigma = 0$. Figure 4 also shows that the curve estimated from (3.10) and (3.11) with $k = 0{\cdot}8$ lies fairly close to, though mostly slightly below, the experimental crosses. This provides an indication that, although some losses may occur for $\Sigma > 0$, they are not severe. It was also noted that in the range of Σ from 0·02 to 0·105, large waves occurred, travelling with the bubble. They can be interpreted as an undular hydraulic jump, occurring after the minimum flow depth has been achieved. According to the arguments given above, jumps of the magnitude observed are unlikely, if the losses ahead of them are appreciable.

The section of the curve labelled H_J in figure 4 was derived from the estimated values of H using the hydraulic jump equation on the flow beneath the bubble for a jump keeping pace with the bubble nose. The equation is

$$H_J = \tfrac{1}{2}H[(1 + 8(F^2/H^3))^{\frac{1}{2}} - 1]. \tag{3.14}$$

The complete curve of H and H_J *versus* Σ makes it clear why the curve of F *versus* Σ with $k = 0{\cdot}8$ in figure 3 terminates at $\Sigma = 0{\cdot}275$.

3.3. *The flow régimes*

The boundaries of the three flow régimes described in § 2 were well defined and a physical reason for them is desirable. A complete explanation cannot be given from the evidence available but the following is worth noting. If (3.10) and (3.11) are solved with $k = 1.0$ it is found that the flow beneath the bubble relative to

the channel wall for $\Sigma < 0{\cdot}027$ is subcritical, with a Froude number less than unity, and is supercritical for larger values of Σ. If the equations are solved with k between 0·8 and 1·0, the flow becomes supercritical at a value of Σ slightly larger than 0·027 but again becomes subcritical at a value of Σ less than unity. Thus it is possible that a hydraulic jump occurs to avoid supercritical discharge over the sill but more accurate information concerning the variation of the radius of curvature of the two-phase interface at the top wall with respect to Σ is required before this conjecture can be properly tested.

The flow régime boundary at $\Sigma = 0{\cdot}105$ may also have been influenced by the difficulties in drainage observed as the blocked condition was approached at $\Sigma = 0{\cdot}368$. It is also worth noting that the flow beneath the bubble relative to the channel wall was laminar for this régime since the Reynolds number, using the depth of flow as a characteristic length, was 500 or less and the basic assumption that the velocity was uniform with depth, used in deriving equations (3.10) and (3.11), is no longer satisfactory.

4. Conclusions

Experimental results have been obtained for the flow of long bubbles in horizontal rectangular channels over a wide range of depths. The hypothesis that the radius of curvature of the bubble nose at the top of the channel does not vary greatly from its value in the situation where the channel is just shallow enough to block the flow explains the experimental results for both rectangular and circular cross-sectioned tubes.

It is stressed that surface tension effects are present even when Σ approaches 10^{-4}. Thus any proposed theoretical treatment of this problem must consider such effects or be restricted to systems of substantial depth, which for the air–water system would be greater than the largest value of 175 mm studied here.

The work was carried out at the Central Electricity Research Laboratories and is published by permission of the Central Electricity Generating Board. Mr C. E. Hagger gave valuable assistance in the experimental part of the work.

REFERENCES

Benjamin, T. B. 1968 *J. Fluid Mech.* **31**, 209.

Bretherton, F. P. 1961 *J. Fluid Mech.* **10**, 166.

Dumitrescu, D. T. 1943 *Z. angew. Math. Mech.* **14**, 42.

Nicklin, D. J., Wilkes, J. D. & Davidson, J. F. 1962 *Trans. Inst. Chem. Engnrs.* **40**, 61.

Runge, D. E. & Wallis, G. B. 1965 NYO-3114-8, *Clearinghouse, Springfield, Va.*

White, E. T. & Beardmore, R. H. 1962 *Chem. Engng Sci.* **17**, 351.

Zukoski, E. E. 1966 *J. Fluid Mech.* **25**, 821.

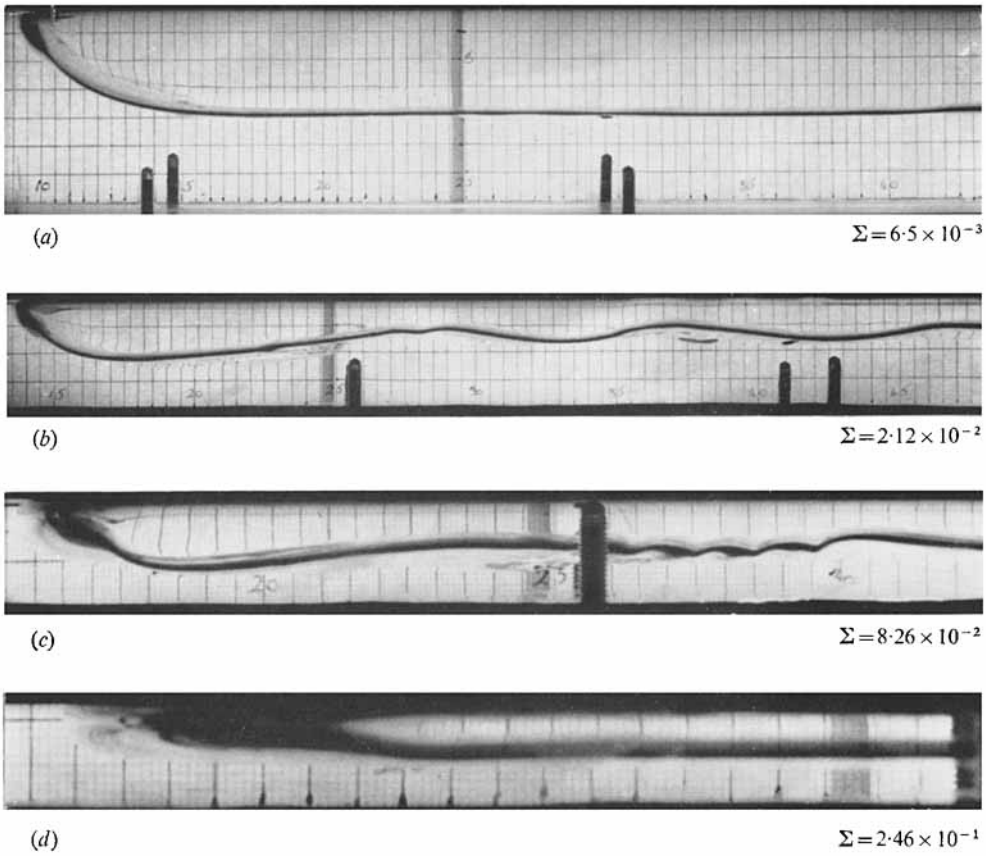

FIGURE 1. Photographs of the bubble.